OV/P-3

Overview of Recent COMPASS Activities

R. Dejarnac[1] and the COMPASS team[1,*]

[1]Institute of Plasma Physics, Czech Academy of Sciences, Prague, Czech Republic

[*] see appendix

E-mail contact of main author: dejarnac@ipp.cas.cz

Abstract. The COMPASS tokamak is one of the present devices operating with an ITER-like plasma shape. Its flexibility due to its small size combined to an extensive set of edge diagnostics and NBI heating allow to address a broad range of key areas in support of the worldwide fusion programme such as H-mode physics, MHD, runaways electrons, disruption studies, plasma-wall interactions. The recent results obtained in COMPASS addressing these key issues are reviewed here.

1. Introduction

The COMPASS tokamak is one of the present devices operating with an ITER-like plasma shape. Its flexibility combined to an extensive set of diagnostics and neutral beam injection heating allow to address a broad range of key areas in support of the worldwide fusion programme such as H-mode, MHD, runaway electrons, disruptions or plasma-surface interaction studies. The recent results obtained in COMPASS addressing these key issues are reviewed here. The control and characterization of the L-H transition and the pedestal physics represent a large part of the COMPASS scientific programme. Recycling and actuators such as the X-point height play a significant role in accessing H-mode. A geodesic acoustic mode oscillating at frequencies 25-40 kHz is observed in L-mode discharges, strongly varying with NBI heating in co- or counter-current injections. COMPASS also contributes to multi-machine databases with pedestal and scrape-off layer (SOL) width scaling studies. Using perturbation coils, the influence of 3D fields on the strike-points splitting, ELM control and transport is reported. The MHD modes studies mainly concern the plasma interaction with Resonant Magnetic Perturbations (RMPs), the characterization of Alfven-like modes and disruption/mitigation experiments. High frequency quasi-coherent oscillations (ranging from 200 kHz to above 1 MHz) that follow Alfvenic frequency scaling are observed in ohmic discharges. An extensive experimental study of MHD effects in losses of runaway electrons has been performed. In the field of disruptions, an inter-machine empirical scaling of critical magnetic disruption precursors has been developed, as well as the study of the disruptions toroidal asymmetry. The exhaust and plasma-material interaction studies in COMPASS contributed to the ITER divertor monoblocks design as part of the International Tokamak Physics Activity (ITPA). Power deposition on leading edge was investigated both experimentally (inner-wall limiters with gaps and leading edges viewed by a high-resolution IR camera) and numerically (particle-in-cell simulations), with the latter reproducing well this experiment. The ITER monoblocks shaping was also investigated in the frame of an ITER contract. Comparison with the deposited power from ion orbit calculations are consistent and confirm results presented at the previous IAEA-FEC by J. P. Gunn et al..

2. The COMPASS tokamak

Since its relocation in the Institute of Plasma Physics of the Czech Academy of Sciences (IPP CAS) in 2006 [1], COMPASS is equipped with new power supply and control systems, two neutral beams injectors (NBI) and an extensive set of diagnostics. All this together, combined with an ITER-like plasma shape, enables to perform ITER relevant studies in different parameter range to the other tokamaks (ASDEX-Upgrade, DIII-D, JET) and to contribute to the ITER scaling.

2.1. Machine description and operation scenarios

The COMPASS tokamak is a compact experimental device ($R = 0.56$ m, $a = 0.2$ m) operating in a divertor plasma configuration with ITER-like plasma cross-section (1 : 10 in linear dimension) [1,2]. The plasma current can go up to 400 kA, the toroidal magnetic field in the range of 0.8–2.1 T, elongation up to 1.8 and different working gases can be used: H, D or He. COMPASS can generate various plasma configurations: circular, elongated or single null X-point (SND) for both toroidal directions of B_T and I_p. The vacuum vessel (VV) of COMPASS is equipped with an open divertor covered by carbon tiles. Two Neutral Beam Injectors operating with deuterium/hydrogen beams ($E_b = 40$ keV, port-through power $P_{NBI} < 0.35$ MW each, pulse length < 0.3 s) are used for additional plasma heating. The beams are injected tangentially (on-axis, co-injection at present). Extensive wall conditioning methods (baking at 150 °C, boronization by carborane vapors in He glow discharge) are used to minimize the deuterium inventory and impurity influx.

Upon its re-installation in IPP Prague, both ohmic and NBI assisted H-modes have been successfully generated after the above mentioned conditioning. In ohmic regime, the H-mode is achieved when the plasma current exceeds approximately $I_P^{LH} \sim 220$ kA (at $B_T = 1.2$ T). The L–H power threshold P_{LH} has a minimum at line-average density in the range of (3.5–4) $\times 10^{19}$ m^{-3}. At these densities the beams of neutral atoms generated by NBIs are already fully absorbed with a negligible shine-through, however, NBI allows to heat plasma also at higher densities. The L–H transition is usually followed either by small Type-III ELMs with frequencies in the range of 400–1500 Hz or ELM-free period. At high plasma currents or in case of NBI-heated plasma, large Type-I ELMs with typical frequency in the approximate range of 80–400 Hz are generated.

2.2. Diagnostics

The COMPASS tokamak is equipped with an extensive set of diagnostics with high temporal and spatial resolution to focus mainly on edge and SOL plasma studies. The core and edge plasma regions are diagnosed using a High Resolution Thomson Scattering (HRTS) system [2,8], based on two Nd:YAG lasers (1.5 J each, 30 Hz) in conjunction with two detection systems, to provides n_e and T_e profiles with a temporal resolution of 60 Hz and a spatial resolution of 3–4 mm in the vertical direction, corresponding to 2–3 mm (~a/100) when mapped to the outer mid-plane (OMP). Fast edge density profiles are measured at OMP using Beam Emission Spectroscopy on Lithium beam operating at 60 keV with 4 μs chopping and spatial resolution ~1 cm and also by using a fast reflectometer in K and Ka bands with $\Delta t \sim 30$ μs. Six arrays of AXUV-based fast bolometers (10 eV < E_{ph} < 10 keV) and two arrays of SXR detectors (1 keV < E_{ph} < 20 keV) provide the tomographic reconstruction of the plasma emissivity with temporal resolution ~1 μs.

A set of 400 magnetic diagnostic coils can provide a full poloidal coverage at several toroidal locations. Local poloidal magnetic fields and their fluctuations are measured by a set

of 16 internal partial Rogowski coils located at one toroidal position and three poloidal arrays of 24 Mirnov coils located at three different toroidal positions. These coils enable poloidally localized measurement of toroidal mode number n in the range of 1–4. Moreover, the tokamak chamber is fully covered by 104 saddle loops that also enable poloidally localized measurements of n in the range of 0–2 (on the low-field side in the range of 0–4). Magnetic data also provide input for the EFIT equilibrium reconstruction.

Visible light is monitored by two fast EDICAM cameras with 450 fps in full-frame (1280 × 1024) up to 116 000 fps in reduced (16 × 16) resolutions. The first camera provides a general view of the plasma configuration (position, shape, wall interaction, etc.) via a tangential view. The second camera is used for monitoring of the divertor region. Additionally, two ultra-fast Photron cameras of APX-RS and SA5 with 3000/7000 fps in full (1024 × 1024) up to 250 kfps (128 × 16) / 1 Mfps (64 × 16) in reduced resolutions are used for observation of fast MHD events (ELM filamentary structure, Beta-induced Alfven Eingenmodes, Geodesic-Acoustic Modes, etc.).

SOL physics is studied using two reciprocating manipulators (one horizontal at OMP and one vertical from the top of the vessel). The horizontal reciprocating manipulator (HRCP) is equipped by an interface compatible with the manipulator at ASDEX Upgrade and allows installation of wide variety of probe heads, such as Retarding Field Analyzer, E×B analyzer or several Langmuir probes (LP) and ball-pen probes (BPP). The Langmuir tips usually measure the floating potential V_{fl} and the ion saturation current I_{sat}, whilst the BPPs, operating in floating mode, provide fast measurements of plasma potential φ_{pl} [3]. It was shown [3] that the difference between the signal of the BPP and the signal of an adjacent floating Langmuir tip is proportional to electron temperature $V_{\mathrm{BPP}} - V_{\mathrm{LP}} = \alpha T_e$. The coefficient $\alpha \approx 2.2$ was found by benchmarking the probe data by HRTS measurements. The principal advantage of T_e measurement by combination of the BPP and floating LP is that the temporal resolution is limited mainly by the sampling frequency of the data acquisition system (5 MHz on COMPASS). Combining density and temperature measurements provide fast measurement of the power flux. The plasma in the divertor region is analyzed by a poloidal array of 39 LPs with a spatial resolution of approximately 5 mm and by an recently installed array of 55 BPPs and 110 LPs, located 135° toroidally away.

3. Edge and SOL physics

3.1. Effect of the X-point height on the L-H transition

It is known that the underlying physics of the access to H-mode is still not fully understood. An empirical scaling law [4] based on global parameters such as density, toroidal field and size of the plasma is the only prediction for ITER to estimate the L- to H-mode power threshold. Recent studies show that other parameters such as recycling, divertor geometry or X-point height play a major role in the access to H-mode. The effects of SOL and divertor conditions on the L-H transition is part of the COMPASS scientific program and experimental output should contribute to the ITPA multi-machine study under the pedestal topical group task PEP-39. In COMPASS, two types of discharges were studies in ohmic regime at constant line-averaged density. A sharp L-H transition is observed in discharges with constant plasma current below the standard COMPASS L-H transition threshold ($I_P < I_P^{LH}$), when the entire plasma column, and thus the X-point is moved from a high (z = +4 cm) to a lower position (z = 0) close to the divertor tile. The L-H transition occurs in the middle of the movement at z = +2 cm and a H-L back transition is observed at the same height when the plasma is moved up from its lower position to its original position in the second part of the discharges. The second type of analyzed discharges are with a constant X-point height with respect to the

divertor tile and with a I_P ramp-up with the starting point $I_P < I_P^{LH}$. A transition to H-mode is observed when the I_P crosses a certain threshold. This threshold is clearly dependant on the height of the X-point as it can be seen on FIG. 1. The ramp-up speed (dI_P/dt) was investigated and seems not to play a major role. However, it is clear that for discharges closer to boronizations (5 days vs. 3 weeks) the L-H power thresholds (P^{LH}) are globally 20% lower. Results for the first type of discharges follow the same trend with a decreasing P^{LH} with decreasing X-point height. Moreover, a 6 kHz mode is observed prior the transition only for the high X-point discharges. This mode occurs 60 ms before the L-H transition and disappears in H-mode. It has been identified as a m/n = 4/(-1) mode in the ion diamagnetic drift direction. This mode is still under investigation.

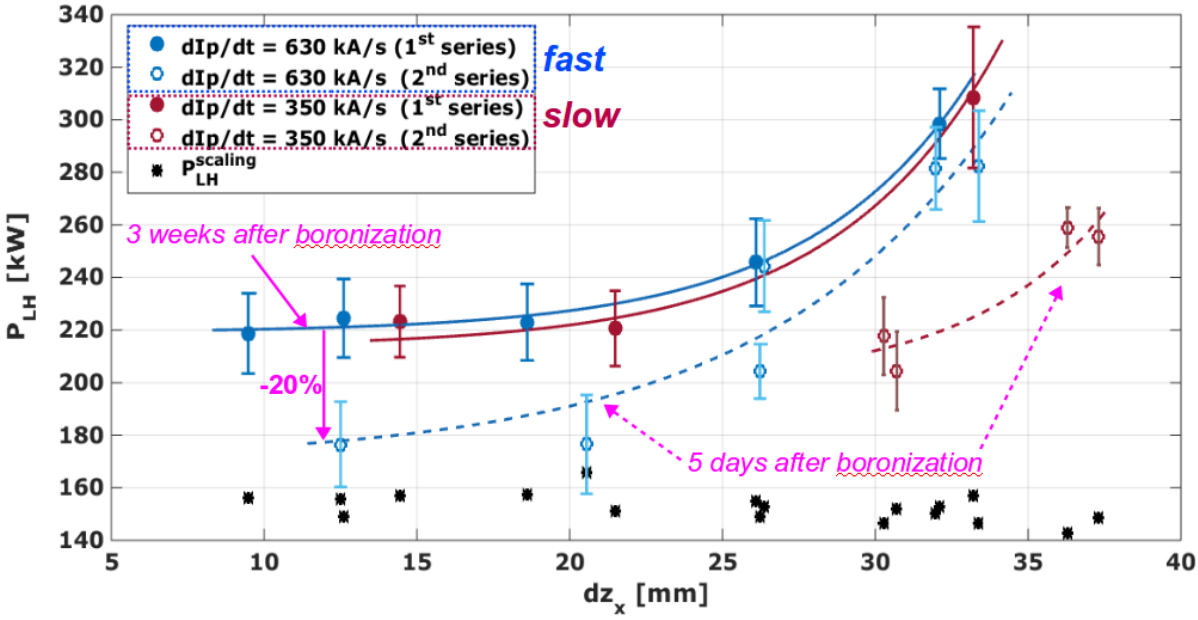

FIG. 1. The L-H power threshold as a function of the X-point height for discharges with plasma at fixed position and with a I_P ramp-up at different speeds and for different wall conditions.

3.2. Study of the Geodesic Acoustic Mode (GAM)

GAM is a turbulence-driven high-frequency branch of zonal flows, which can play a role in self-regulation of turbulent transport by shear decorrelation of turbulent structures. On COMPASS, electrostatic as well as magnetic component of GAM oscillations has been recently identified [5] and characterized in Ohmic and L-mode discharges. The frequency of the mode has been found in the range 25-40 kHz in diverted plasmas and 40-50 kHz in limited plasmas. The mode exhibits non-local structure with frequency constant over radial extent of at least several centimetres inside LCFS, i.e. the region accessible by reciprocating probes. With additional NBI heating, GAM frequency increases proportionally to edge ion sound speed. However, GAM amplitude changes as well, differently for co-current (CO) and counter-current (CNT) injection (see FIG. 2, I_p = 180 kA, n=4x10^{19} m^{-3}, q_{95}=3.7). While the GAM amplitude is strongly suppressed during CO-NBI, the mode is enhanced during CNT-NBI. This behavior somewhat resembles observations on JT-60U [6]. The mechanism of GAM suppression or excitation by NBI on COMPASS is currently not clear, but it could be related to a change of toroidal plasma flow and parallel current by NBI as suggested in [7]. Except oscillations of plasma and floating potential the mode exhibits also small oscillations of local electron temperature in the order of ~1 eV. Radial wave length of the potential is found λ_r~3 cm and the mode propagates radially outwards with velocity ~ 0.5 km/s.

The mode creates fluctuations of the radial electric field δE_r~1.5-2.5 kV/m. This corresponds to amplitude of poloidal ExB velocity fluctuations in the order of δv_p ~2-3 km/s, i.e. ≥30% of maximal magnitude of edge poloidal velocity, but locally it can reach up to $v_{p,GAM}/\langle v_p \rangle \sim 1$. The shearing rate of GAM-induced flows has been estimated as $\omega_{ExB} = |\partial E_{r,GAM}/\partial r| \approx 5 \cdot 10^5 s^{-1}$. In diverted discharges the mode creates strong axi-symmetric magnetic oscillations both in radial and poloidal components of the field, exhibiting standing wave structure in the poloidal direction. Compared to m = 2 structure of magnetic field predicted for ideal circular plasma the shaping seems to induce additional Fourier components.

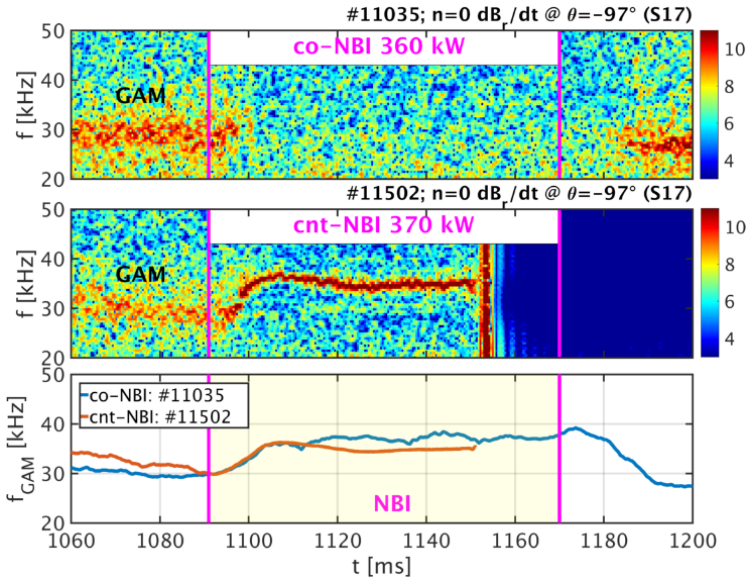

FIG. 2. Spectrogram of n=0 dBr/dt fluctuations in the divertor region showing frequency and amplitude of GAM magnetic component during co-NBI (a) and cnt-NBI (b) heating. GAM frequency estimated by Hilbert transform is compared for both cases in (c). Discharge #11502 ended with disruption at 1153 ms.

3.3. Pedestal scaling studies

In the first experimental campaign focused on pedestal scaling, HRTS was used to measure profiles in the last 20% of ELM cycle in a series of ELMy H-mode discharges (both Ohmic and NBI-assisted) with varying plasma current between 160 and 330 kA. ELMs were detected using divertor H-alpha signal and only those with $P_{sep} > 40$ kW/m^2 qualified as Type I ELMs [9]. The profiles were fitted using a modified hyperbolic tangent function [10] to obtain the pedestal widths and heights. These were then translated to pedestal dimensionless parameters $\beta_{e,ped}^{pol}$, υ^*_{ped} and ρ^*_{ped} (for their definitions see [11]) using assumption of $T_i = T_e$ in the pedestal region. The ranges of the dimensionless parameters are compared to values obtained in the JET & DIII-D Identity experiment [11]. The experimental results are generally not far from those achieved in the identity experiment, however it was not possible to match all parameters into the desired range at once. Twenty three selected measured pedestals on COMPASS were reproduced using the EPED model and used to complement predictions for 5 other tokamaks [12] (see FIG. 3).

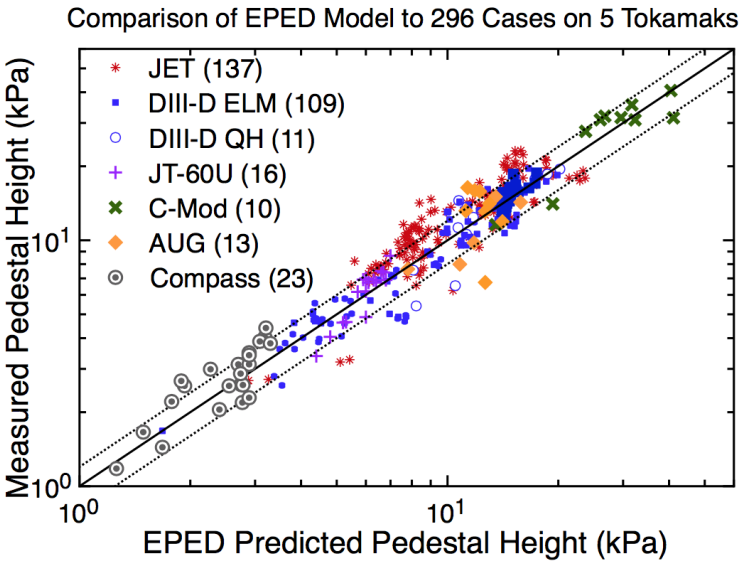

FIG.3. Measured pedestal height in multi-machine experiments (including the 23 COMPASS selected discharges) compared to EPED predictions.

3.4. Resonant magnetic perturbation (RMP) studies

COMPASS is equipped with a rich set of coils for producing magnetic perturbations with a four-fold symmetry (maximum toroidal mode number n=2) [13]. Magnetic perturbation experiments on COMPASS have been performed with two even parity n=2 coil configurations: two rows of off-midplane coils and three rows with an additional large midplane coil. The configuration with the large midplane coil was found to be more susceptible to the formation of a 3/2 locked mode, which sometimes led to a disruption. Most of the experiments were performed in ohmic L-mode. During the application of the resonant magnetic perturbation a clear splitting of the outer strike point was observed using a visible spectrum camera and using an array of divertor probes (measuring in floating potential, ion saturation current and sweeping modes). The observed secondary peaks of ion saturation current are found to be correlated with the peaks of floating potential (FIG. 4, LEFT). The magnetic response measured with a high poloidal resolution using saddle loops [14] and footprint data from probes and visible camera show no signs of a threshold or nonlinear behavior in the shots without the locked mode formation. In particular, the strike point spitting appears gradually in shots with a slow ramp of the RMP field and the measured magnetic response is always linearly proportional to the applied RMP field. FIG. 4, RIGHT shows that the plasma response field measured outside the plasma is in opposite spatial phase to the original RMP perturbation, at magnitude one order lower for both the experimental measurement and the model. Whilst simulations [14] using the MARS-F code successfully reproduce the response field at $\theta \approx \pm 0.4\,\pi$, there is a discrepancy at $\theta \approx 0$ position. Moreover, it has been observed that the θ profile shape of the measured response field is very similar for both RMP coil configurations, which also had similar features of strike point splitting in L-mode. In ohmic H-mode, the perturbations led to an increase of the ELM frequency, apparently explained by density pump-out. The off-midplane configuration was used here, as the configuration with the large midplane coil was too susceptible to disruptions. Some signs of strike point splitting were also observed in H-mode, again without any threshold or nonlinear behavior.

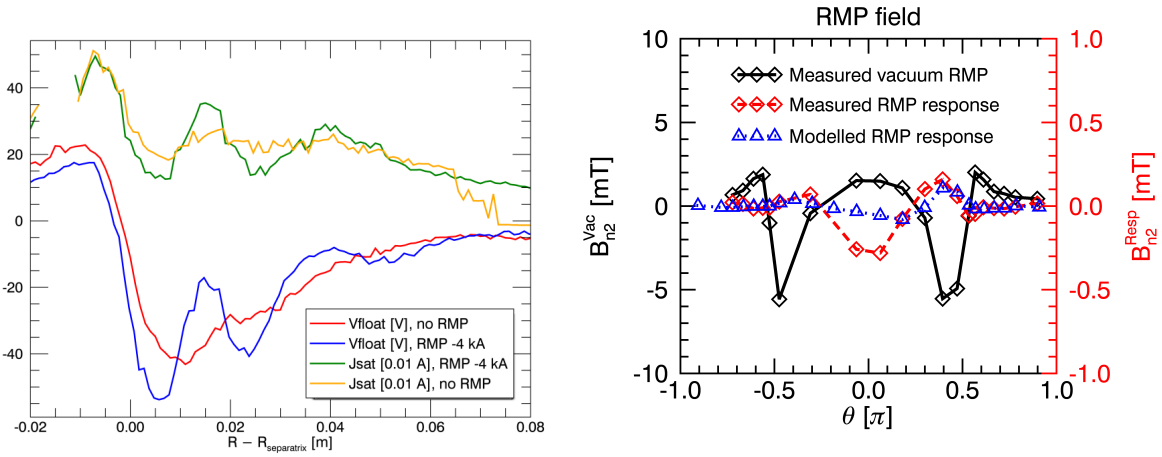

FIG. 4. LEFT: Floating potential (V_{float}) and ion saturation current (J_{sat}) on the COMPASS outer divertor measured by the Langmuir probe array as a function of the distance to the separatrix (i.e. the original strike point calculated by equilibrium reconstruction) in shots with and without resonant magnetic perturbation. RIGHT: Poloidal profile of n=2 RMP field on COMPASS. Black (left) axis and data – measurement of original RMP perturbation. Red axis (right), red and blue data – measurement and model of plasma response field.

4. Core physics and quasi-coherent modes

4.1. Studies of Alfven Eigenmode oscillations

Utilizing the inside vessel Mirnov coils and data acquisition system with good transmission properties, we have observed High-Frequency (HF) plasma oscillations up to 2.5 MHz, on various poloidal positions and in different plasma regimes of the tokamak COMPASS. Specifically, ELM-free H-mode discharges at higher densities are typically associated with multitude of coherent oscillation modes on LFS at the same time, in the frequency range of 50-150 kHz. Their respective *m* and *n* mode numbers are increasing function of frequency, the modes have been also detected in plasma potential measurements using HRCP and are perturbed by ELM activity, while sawtooth activity only slightly modulates their frequency. Using linear MHD model KINX, these oscillations have been identified as Beta-induced Alfven Eigenmodes. Similar oscillations are observed at the same time on HFS, in the frequency range 150-250 kHz. These are, however, of quasi-coherent character (i.e. wide band slightly above noise level) and exhibit different frequency scaling to the LFS oscillations. Using KINX simulations and taking their other properties into account, we have identified them as Toroidal Alfven Eigenmode oscillations. It should be noted, however, that the oscillations appear in both NBI-assisted and ohmic H-modes and their exact excitation mechanism is thus not understood at the moment.

Furthermore, more bands of quasi-coherent oscillations appear on HFS, with frequencies up to 1 MHz in both L-mode and H-mode, regardless of the used heating scheme. Oscillations last typically over the most of the discharge duration and their frequency scaling follows that of Alfven Eigenmodes, with respect to both their temporal evolution during single discharge and multi-discharge comparison (FIG. 5). Hence they are referred to as *Long-lived Alfven oscillations*. They bear many similarities to previously-reported plasma oscillations on TFTR (such as mode amplitude scaling, amplitude suppression by L-H transition, band structure) [15] and on AUG (such as electron-diamagnetic drift rotation, $n = 1$ structure) [16] implying their possible excitation mechanism on COMPASS might be coupling of the drift wave turbulence to the ordinary Alfven wave spectrum at cold plasma edge.

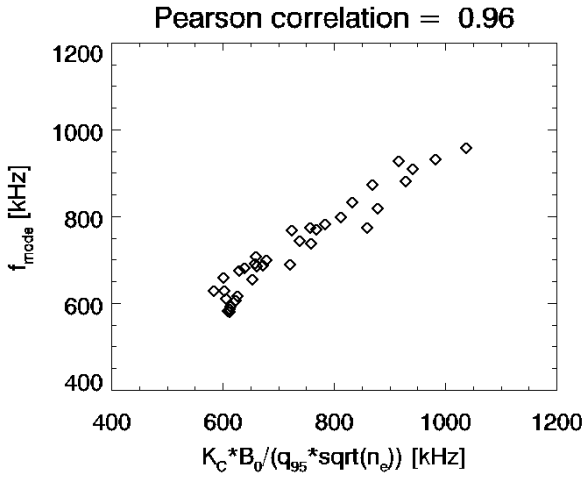

FIG. 5. Comparison of Long-lived Alfven oscillation frequency to the Alfven eigenmode scaling relation, across multiple discharges. B_0 is toroidal magnetic field, n_e line-averaged electron density and K_c parameter is function of plasma composition.

During low-density discharges with high runaway electron activity, chirped plasma oscillations in frequency range 800-2500 kHz can be observed on LFS. Their bursting, chirping behavior, coherent character and short (~10^1 ms) duration distinguish them apart from Long-lived Alfven oscillations and hence they are referred to as *chirping modes*. Nevertheless, they too follow Alfven Eigenmode frequency parametric scaling, which together with their HF points towards the Alfvenic character, despite the fact they are present in both NBI-heated and ohmic plasmas. The onset of these modes is typically accompanied with a significant X-ray spike, while the chirping bursts themselves are correlated with sawtooth crashes. This implies that possible excitation of the modes might be due to internal reconnection events.

4.2. Runaway electron (RE) studies

Runaway electron studies present another important contribution of the COMPASS tokamak experimental programme. Indeed, post-disruption RE beam can be highly localised so that it could severely damage plasma facing components and blanket modules of fusion reactors, including ITER. In recent dedicated experiments at COMPASS a post-disruption RE beam was successfully produced in Argon initiated disruption of the current ramp-up phase of the plasma discharge, see FIG. 6. This is a significant result, for it will allow for important experiments on RE control and mitigation. For details see [17]. Moreover, the new wide-angle fast visible camera considerably enhanced understanding of the RE beam generation after the Argon triggered disruption in COMPASS, see FIG. 7. In particular, the observed initial formation of the filamentary structures present a novel result which deserves attention. In experiments focused on RE confinement in COMPASS plasmas (i.e. no disruption, low density plasmas, ne ~ 2-3.10e19 m-3) relation between plasma MHD activity and RE loss was studied. A strong correlation between MHD instabilities (measured by rich magnetic diagnostic of COMPASS) and RE losses (determined via increase in HXR signal) was demonstrated. For more information on this topic see [18]. Considerable attention is also dedicated to experimental benchmarking of RE models under development, in particular the LUKE Fokker-Planck solver of the RE generation.

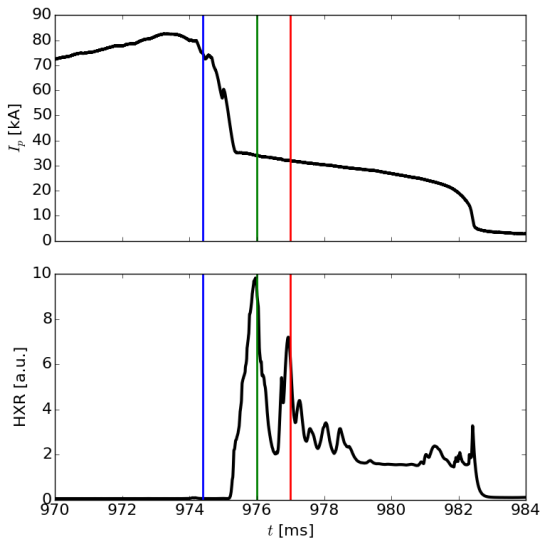

FIG. 6. Top: Evolution of the plasma current in COMPASS discharge #12202 with Ar puff at 973ms. A clear RE beam current plateau is formed after the plasma current quench, approx. from 975ms to 982ms. Bottom: Hard X-ray (HXR) radiation measured by a monitoring NaI(Tl) scintillation detector. HXR is generated by RE collisions with the tokamak inner wall. The three vertical lines specify times corresponding to the fast camera pictures presented in FIG. 7.

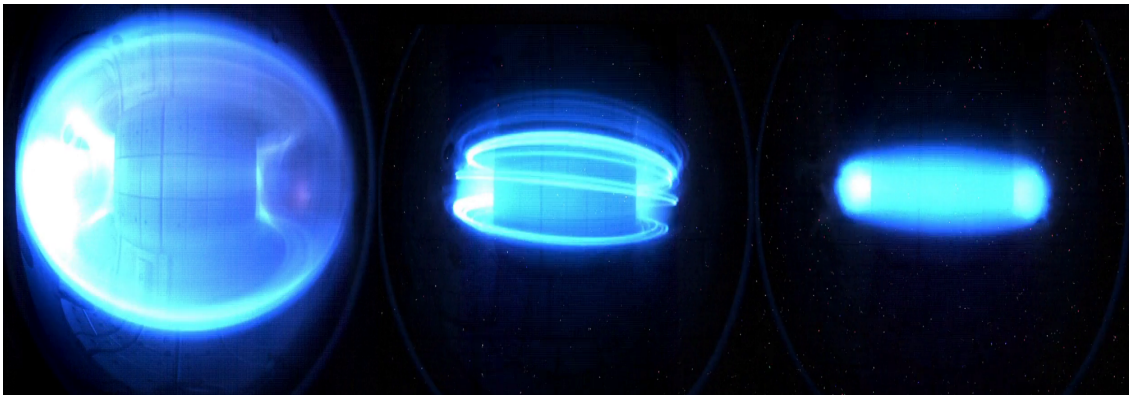

FIG. 7. Three frames from the wide-angle fast visible camera (real colors), COMPASS discharge #12202 with Ar puff at 973ms. From left to right: t=974.4ms (blue line in FIG. 6) Ar light from the plasma edge at the beginning of the disruption; t=976.0ms (green line in FIG. 6) RE beam formation with clear filamentary structure ; t=977.0ms (red line in FIG. 6) plateau phase of the RE beam.

5. Plasma-surface interactions

5.1. Particle-in-cell (PIC) simulations of heat loads on ITER W divertor monoblocks

In support of the ITER W divertor monoblock shaping decision, PIC simulations of plasma deposition on ITER divertor monoblocks have been performed for both inner (IVT) and outer vertical targets (OVT), including poloidal (PG) and toroidal gaps (TG). Results are given for misaligned, flat and shaped monoblocks during and in between ELMs. This work was done in the frame of an IO contract. The main objective of the simulations was to asses the role of local electric fields on the power flux distribution, which were not taken into account in a previous study of the problem (in order to simplify and accelerate the calculations) using Monte Carlo ion orbit calculations (IOC) [19]. PIC output demonstrate that even if in some cases the electric field plays a distinct role, when heat diffusion into the bulk material is taken into account, the results are very similar to those obtained using as input the power load

distribution from IOC. This is a consequence of the small spatial scales over which the ion orbits distribute the power, but the key result of this study is that the computationally much less intensive IOC can be used with confidence in monoblock shaping design. Results of PG simulations for steady-state and slow transient plasma conditions show that due to finite Larmor effects, the leading edge (LE) created by the radially misaligned tile receives lower heat flux than predicted by the optical approximation (OA). However, the heat flux that is missing on the LE is redistributed on the top surface of the monoblock within 1-2 millimetres from the edge. The integral heat flux arriving to the monoblock is not changed (proving that the calculation respects energy balance) and due to heat diffusion inside the material the effect on monoblock temperature is negligible. That is, exposed LEs suffer overheating whether the heat flux is highly concentrated as given by the OA, or somewhat smoothed due to Larmor radius effects. The results are in a good agreement with IOC. Results of toroidal gap simulations for ELMy plasma conditions show again a good agreement with the IOC. In case of IVT monoblocks, both models significantly deviate from the simple OA. The PIC and ion orbit codes predict highest ELM heat flux deposition on the plasma shadowed side of the monoblock, whereas the OA anticipates zero flux. In case of OVT all models predict deposition at the plasma wetted side, however PIC and ion orbit models predict significant peaking of the heat flux close to the monoblock edge, which is due to a preferred direction of ion gyration. The heat flux at the edge can in some cases exceed the melting threshold for tungsten. The PIC model also predicts peaking of electron heat flux, which was not foreseen by the ion orbit code as it did not trace electrons. The resulting heat flux received by the monoblock edge does not change on a spatial scale relevant to heat diffusion during ELMs, however the fact that the heat flux is deposited by electrons and not by ions may have influence on the material response. Result of optical hot spot simulation shows that the heat flux propagation down the toroidal gap onto so-called "optical hot spots" is attenuated due to finite Larmor effects. Here again the PIC results are in a good agreement with ion orbit code outputs. We can conclude that the role of electric fields in the sheath on the heat flux distribution on the monoblocks is negligible and therefore IOC are suitable to study this problem.

5.2. Power deposition on leading edges in support of ITER W monoblock shaping

The numerical study presented in section 5.1 has been followed by an experimental one on COMPASS in the frame of the ITPA DSOL-31 task. Heat loads on misaligned edges are investigated using a dedicated inner wall limiter (IWL), specially designed to present ITER relevant LE heights and incident angles between the field lines and the top surface, see FIG. 8. The IWL is made of graphite and has a roof-shape with a slope of 2.5°. The central tile includes four regions, with each region presenting a poloidally running gap and a LE with a fixed misalignment, *h*. The misalignment is different for each region, *h = 0, 0.3, 0.6, 0.9 mm* anti-clockwise from region #1, covering both the typical maximum misalignment (~0.3 mm) expected on ITER in region #2 and the value used in the 2013 JET melting experiment (~1.0 mm) in region #4. In order to recreate the JET melting experimental set-up, where 8 lamellas before the protruding lamella were recessed to avoid any shadowing, the region #3 presents a closed pocket before the LE to develop a mini-SOL. IWL ohmic discharges with I_P = 130 kA and B_t = 0.9 T (yielding Q^{perp} ~1 MW.m^{-2}) are used with the plasma contact point leaning on the different regions of interest of the central tile on a shot-to-shot basis during 150 ms steady-state. The IWL is in direct view of a high resolution IR camera (0.3mm/pixel) and experimental surface temperature profiles, $T^{surf,IR}$, are compared to synthetic data from 2D FEM thermal calculations using the CAST3M code convoluted with a modulation transfer function specific to the camera, allowing direct comparison with the experimental IR profiles.

The comparison between the experiment ($T^{surf,IR}$) and the simulation using the OA ($T^{surf,OA}$) is done for the COMPASS discharge #11620 with the plasma contact point covering both regions #2 and #3, see FIG. 8, BOTTOM. A very good qualitative and quantitative agreement (less than the measurements error of 10%) is observed between $T^{surf,OA}$ and $T^{surf,IR}$ both on the temperature decay and at the peak for the two simulated LEs. On region #3, the IR profile is well reproduced by the simulation despite the mini-SOL. The temperature drop due to the magnetic shadow inside the mini-SOL is also well reproduced.

The two main conclusions that we can draw from such results is that 1) the OA is a valid approach to describe the power deposition on small LEs with grazing incident angles and 2) the mini-SOL in front of the LE is not responsible for any power mitigation in the present COMPASS experiment as it was observed in JET. Indeed, no mitigation factors have to be applied in any case to the OA description of power fluxes around LEs to match $T^{surf,IR}$. The recessed volume before the misaligned edge does not affect the power falling on it. Power deposition profiles around LEs in PGs have also been calculated from PIC calculations. They show a smoothing of the power on the LE side due to the ion Larmor gyration and a downstream enhanced flux on the LE top, toroidally spread, conserving the power balance. For a small LE ($h = 0.6\ mm$) and under the assumption of ambipolarity implemented in the PIC code, the predicted power flux profiles do not match the IR measurements. The peak temperature at the LE corner is significantly lower and the temperature decay is slower than the experimental one. This result tends to show that the power is not dominated by ions but more by electrons. Arbitrary changing the composition of the total power profile in order to have most power carried by electrons show a better agreement with experimental data.

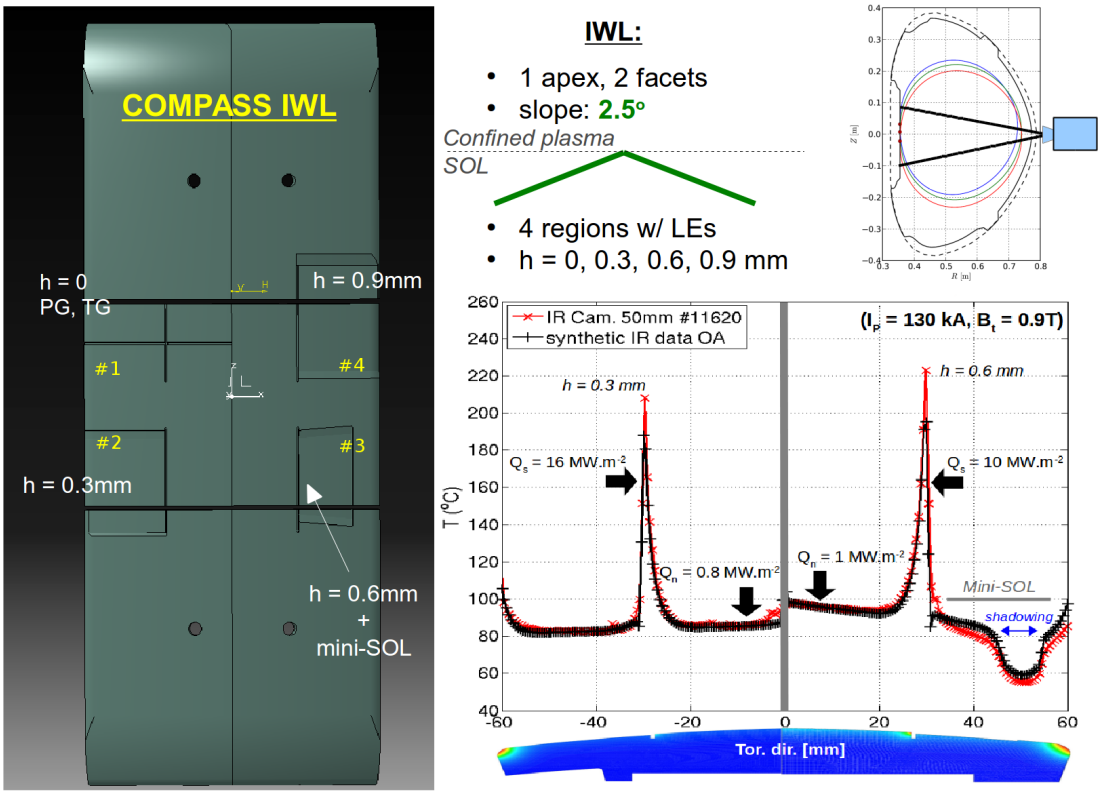

FIG. 8. LEFT: CAD drawing of the COMPASS IWL. TOP: Schemes of the limiter cross-section (left) and of the experimental set-up (right). BOTTOM: Surface temperature profiles along regions #2 & #3 (red x: experiment, black +: synthetic data using OA).

Acknowledgement: This work has been carried out within the framework of the EUROfusion Consortium and has received funding from the Euratom research and training

programme 2014-2018 under grant agreement No 633053. The views and opinions expressed herein do not necessarily reflect those of the European Commission. This project was supported by the MEYS project LM2015045 and by national grants GA 14-35260S, GA 16-25074S, GA 16-24724S.

References:

[1] PANEK, R., et al., "Reinstallation of the COMPASS-D tokamak in IPP ASCR", Czech. J. Phys. **56** (2006) B125.

[2] AFTANAS, M., et al., "High-resolution Thomson scattering system on the COMPASS tokamak: Evaluation of plasma parameters and error analysis", Rev. Sci. Instr. **83** (2012) 10E350.

[3] ADAMEK, J., et al., "Ball-pen probe measurements in L-mode and H-mode on ASDEX Upgrade", Contrib. Plasma Phys. **50** (2010) 854.

[4] MARTIN, Y. R., et al., "Power requirement for accessing the H-mode in ITER", 11th IAEA Technical Meeting on H-mode Physics and Transport Barriers, J. of Physics: Conf. Series **123** (2008) 012033.

[5] SEIDL, J., et al., "Observation of geodesic acoustic mode-like oscillations on COMPASS", Proceedings of the 42nd EPS Conference, P4.103.

[6] MATSUNAGA, G., et al., Proceedings of the 39th EPS Conference, P2.062 (2012).

[7] ELFIMOV, A. G., et al., "Geodesic mode instability driven by the electron current in tokamak plasmas", Phys. Letters **A 378**, (2014) 800-804.

[8] BOHM, P. et al., "Edge Thomson scattering diagnostic on COMPASS tokamak: Installation, calibration, operation, improvements", Rev. Sci. Instr. **85** (2014) 11E431.

[9] PANEK, R. et al., "Status of the COMPASS tokamak and characterization of the first H-mode", Plasma Phys. Control. Fusion **58** (2016) 014015.

[10] STEFANIKOVA, E. et al., "Fitting of the Thomson scattering density and temperature profiles on the COMPASS tokamak", Rev. Sci. Instr. **87** (2016) 11E536.

[11] FRASINETTI, L. et al., "Spatial resolution of the JET Thomson scattering system", Rev. Sci. Instr. **83** (2012) 013506.

[12] SNYDER, P. B. et al., "A first-principles predictive model of the pedestal height and width: development, testing and ITER optimization with the EPED model," Nucl. Fusion **51** (2011) 103016.

[13] CAHYNA, P. et al., "The optimization of resonant magnetic perturbation spectra for the COMPASS", Nucl. Fusion **49** (2009) 055024.

[14] MARKOVIČ, T. et al., "Measurements and modelling of plasma response field to RMP on the COMPASS tokamak", Nucl. Fusion **56** (2016) 092010.

[15] CHANG, Z., et al., "Alfven frequency modes at the edge of TFTR plasmas", Nuclear Fusion **35** (1995) 1469.

[16] MARASCHEK, M., et al., "Observation of Toroidicity-Induced Alfven Eigenmodes in Ohmically Heated Plasmas by Drift Wave Excitation", Phys. Rev. Letters **79** (1997) 4186.

[17] VLAINIC, M. et al., "Post-disruptive runaway electron beams in the COMPASS tokamak", J. Plasma Phys. **81**, (2015) 475810506.

[18] MLYNAR, J. et al., "Losses of runaway electrons in MHD-active plasmas of the COMPASS tokamak", Proc. 26th IAEA Fusion Energy Conference, Kyoto, Japan (2016).

[19] GUNN, J. P. et al., "Surface Heat Loads on Tungsten Monoblocks in the ITER Divertor", Proc. 25th IAEA Fusion Energy Conference, St Petersburg, Russia (2014).

Appendix: The COMPASS team

I. Abramovic[23], J. Adámek[1], M. Aftanas[1], G. Anda[13], M. Becoulet[15], A. Bencze[13], M. Berta[1,14], P. Bílková[1], O. Bogár[1], P. Böhm[1], P. Cahyna[1], D. Carralero[3], J. Cavalier[1], J. Čeřovský[4], S. Costea[8], M. De Angeli[20], G. De Temmerman[21], R. Dejarnac[1], A. Devitre[9], M. Dimitrova[1], R. Duban[4], D. Dunai[13], I. Ďuran[1], S. Entler[1], M. Farník[4], A. Fassina[11], H. Fernandes[7], O. Ficker[1,4], L. Frassinetti[6], E. Gauthier[15], S.N. Gerasimov[12], O. Grover[4], P. Háček[1,2], E. Hasan[5], J. Havlíček[1], A. Havránek[1], C. Hidalgo[1], J. Horáček[1], M. Hron[1], O. Hronova[1], M. Imríšek[1,2], C. Ionita[8], M. Jakubowski[22], F. Janky[1], K. Jiráková[4], M. Jirsa[1], A. Kendl[8], V. Klevarova[2], M. Komm[1], A. Kostic[10], K. Kovařík[1,2], J. Krbec[1,4], L. Kripner[1,2], L. Krlín[1], V. Löffelmann[4], J. Loureiro[7], E. Macúšová[1], T. Markovič[1,2], E. Martines[11], J. Matejicek[1], M. Matušů[4], H. van der Meiden[18], A. Melnikov[19], K. Mitošinková[1,2], J. Mlynář[1], T. Morgan[18], D. Naydenkova[1,2], C. Norscini[1], R. Pánek[1], R. Papřok[1,2], P. Pavlo[1], M. Peterka[1,2], J. Písačka[1], V. Plyusnin[7], A. Podolník[1,2], Tsv. Popov[5], J. Preinhaelter[1], M. Rabinski[22], S. Ratynskaia[6], D. Refy[13], P. Ricci[17], R. Scannell[12], R. Schrittwieser[8], J. Seidl[1], A. Seman[4], M. Siles[4], C. Silva[7], M. Šos[1,4], M. Spolaore[11], E. Štefániková[1,2], J. Stöckel[1], J. Svoboda[4], P. Tamain[15], M. Tomeš[1,2], J. Urban[1], G. Van Oost[10], J. Varju[1], M. Vilemova[1], M. Vlainic[1,10], P. Vondráček[1,2], V. Weinzettl[1], J. Zajac[1], F. Žáček[1], H. Zohm[3], S. Zoletnik[13]

[1] Institute of Plasma Physics, Prague, Czech Republic
[2] Faculty of Mathematics and Physics, Charles University in Prague, Czech Republic
[3] Max-Planck-Institut für Plasmaphysik, Garching, Germany
[4] Faculty of Nuclear Sciences and Physical Engineering, CTU, Prague, Czech Republic
[5] Faculty of Physics, St. Kliment Ohridski University of Sofia, Sofia, Bulgaria
[6] KTH Royal Institute of Technology, Stockholm, Sweden
[7] Instituto de Plasmas e Fusão Nuclear, Instituto Superior Técnico, Universidade de Lisboa, Lisboa, Portugal
[8] Institute for Ion Physics and Applied Physics, University of Innsbruck, Innsbruck, Austria
[9] Universidad de Costa Rica, San José, Costa Rica
[10] Department of Applied Physics, Ghent University, Belgium
[11] Consorzio RFX, Padua, Italy
[12] CCFE, Culham, United Kingdom
[13] Institute for Particle and Nuclear Physics, Wigner RCP, HAS, Budapest, Hungary
[14] Széchenyi István University, Gyor, Hungary
[15] CEA Cadarache, France
[16] CIEMAT Madrid, Spain
[17] EPFL Lausanne, Switzetland
[18] DIFFER, Netherlands
[19] National Research Centre 'Kurchatov Institute', Moscow, Russia
[20] Instituto di Fisica del Plasma - CNR, Milano, Italy
[21] ITER Organization, St. Paul-lez-Durance, France
[22] NCBJ, Swierk, Poland
[23] Eindhoven University of Technology, The Netherlands